



1 **A lab in the field: High-frequency analysis of water quality** 2 **and stable isotopes in streamwater and precipitation**

3 Jana von Freyberg^{1,2}, Bjørn Studer¹, James W. Kirchner^{1,2}

4 ¹Department of Environmental Systems Science, ETH Zurich, Zurich, Switzerland

5 ²Swiss Federal Research Institute WSL, Birmensdorf, Switzerland

6 *Correspondence to:* Jana von Freyberg (jana.vonfreyberg@usys.ethz.ch)

7 **Abstract.** High-frequency measurements of solutes and isotopes (¹⁸O and ²H) in rainfall and streamflow can
8 shed important light on catchment flow pathways and travel times, but the workload and sample storage artifacts
9 involved in collecting, transporting, and analyzing thousands of bottled samples severely constrain catchment
10 studies where conventional sampling methods are employed. However, recent developments towards more
11 compact and robust analyzers have now made it possible to measure chemistry and water isotopes in the field at
12 sub-hourly frequencies over extended periods. Here we present laboratory and field tests of a membrane-
13 vaporization continuous water sampler coupled to a cavity ring-down spectrometer for real-time measurements
14 of δ¹⁸O and δ²H, combined with a dual-channel ion chromatograph (IC) for synchronous analysis of major
15 cations and anions. The precision of the isotope analyzer was typically better than 0.03‰ for δ¹⁸O and 0.17‰
16 for δ²H, for 10min average readings taken at intervals of 30min. Carryover effects were less than 1.2% between
17 isotopically contrasting water samples for 30min sampling intervals, and instrument drift could be corrected
18 through periodic analysis of secondary reference standards.

19 We tested the coupled isotope analyzer / IC system under field conditions by analyzing streamwater and
20 precipitation every 30min over 28 days in a small catchment. These high-frequency measurements facilitated a
21 detailed comparison of event-water fractions via end-member mixing analysis with both chemical and isotope
22 tracers. For two events with relatively dry antecedent moisture conditions, event-water fractions were <20%
23 based on isotope tracers, but were significantly overestimated (39% to 83%) by the chemical tracers. These
24 observations, coupled with the storm-to-storm patterns in precipitation isotope inputs and the associated
25 streamwater isotope response, led to a conceptual hypothesis for runoff generation in the catchment. Under this
26 hypothesis, the pre-event water that is mobilized by precipitation events may, depending on antecedent moisture
27 conditions, be significantly shallower, younger, and less mineralized than the deeper, older water that feeds base
28 flow and thus defines the "pre-event" end-member used in hydrograph separation. This proof-of-concept study
29 illustrates the potential advantages of capturing isotopic and hydrochemical behavior at high frequency over
30 extended periods that span multiple hydrologic events.

31 **1. Introduction**

32 Environmental tracers are widely used in hydrology to investigate recharge processes, subsurface flow
33 mechanisms and streamflow components (Leibundgut and Seibert, 2011). The most common environmental
34 tracers are the naturally occurring stable water isotopes ¹⁸O and ²H (Klaus and McDonnell, 2013). Solutes such
35 as dissolved organic compounds, nutrients, and major ions are also widely used, together with stable isotopes, as
36 indicators of flowpaths and biogeochemical reactions (e.g., McGlynn and McDonnell, 2003; Vitvar and
37 Balderer, 1997; Weiler et al., 1999). Environmental tracer studies typically involve manual or automated



38 sample collection, followed by transport, storage, and subsequent laboratory analysis. The time and effort
39 involved in sample handling are often a major constraint limiting the frequency and duration of sampling, and
40 thus the scope of tracer studies.

41

42 To date, isotope studies have maintained high sampling frequencies only during a few storm events (e.g.,
43 Berman et al., 2009; Lyon et al., 2008; Pangle et al., 2013), with the result that only limited ranges of catchment
44 behavior have been explored. Long-term catchment studies capture a wider range of hydrologic events, but
45 generally collect water samples at only weekly or monthly intervals for subsequent laboratory analysis (e.g.,
46 Buso et al., 2000; Darling and Bowes, 2016; Jasechko et al., 2016), making higher-frequency behaviors
47 unobservable. As pointed out by Kirchner et al. (2004), sampling at intervals much longer much smaller than
48 the hydrological response times of a catchment may result in significant losses of information. For instance,
49 sub-daily sampling is required to capture diurnal fluctuations in streamwater hydrochemistry, which reflect in-
50 stream biological activity (e.g., Hayashi et al., 2012; Rode et al., 2016b). Thus, high-frequency sampling can
51 help to determine ecological effects or to identify biogeochemical hot spots and hot moments, which are
52 characterized by disproportionately high reaction rates (e.g., McClain et al., 2003; Vidon et al., 2010). In order
53 to differentiate hydrological and biogeochemical catchment processes related to different water ages and flow
54 pathways, long-term monitoring has to be complemented by additional high-frequency hydrochemical and
55 isotope measurements. So far, only a few long-term studies have sampled streamwater at daily or sub-daily
56 intervals for on-site measurements or subsequent analysis in the laboratory, such as at Plynlimon, Wales (Neal
57 et al., 2011), at the Kervidy-Naizin catchment in western France (Aubert et al., 2013) or at the Selke river in
58 Germany (Rode et al., 2016a). Such studies have yielded fundamental insights into catchment hydrological
59 behaviour, not only at a wide range of temporal scales but also under varying hydro-climatic conditions (e.g.,
60 Benettin et al., 2015; Halliday et al., 2013; Harman, 2015; Kirchner and Neal, 2013; Riml and Worman, 2015).

61

62 The recent development of compact and robust isotope analyzers has fostered initial attempts to continuously
63 measure $\delta^{18}\text{O}$ and $\delta^2\text{H}$ in streamwater or precipitation directly in the field. The only previous field-based
64 isotope monitoring of 4 contiguous weeks was carried out by Berman et al. (2009) with a customized liquid
65 water isotope analyzer based on off-axis integrated cavity output spectroscopy (OA-ICOS; Los Gatos Research,
66 Mountain View, CA, USA), which measured $\delta^{18}\text{O}$ and $\delta^2\text{H}$ in 90 samples per day. As the system was based on
67 repeated injections of samples into a vaporizer, daily maintenance (i.e., injection septa change, filter cleaning)
68 was required to keep it running. An alternative approach uses a semi-permeable membrane to generate water
69 vapor from a continuous sample throughflow, which is then transferred to a wavelength scanned – Cavity Ring-
70 Down Spectrometer (CRDS) (e.g., Herbstritt et al., 2012). Munksgaard et al. (2011) developed such a custom-
71 made diffusion sampler and attached it to a CRDS (Picarro Inc., Santa Clara, CA, USA) to measure $\delta^{18}\text{O}$ and
72 $\delta^2\text{H}$ in precipitation at frequencies of up to 30s over a 15day period (Munksgaard et al., 2012).

73

74 A similar diffusion sampling system has recently become commercially available (Continuous Water Sampler
75 Module, or CWS; Picarro Inc., Santa Clara, CA, USA), which allows for quasi-continuous measurements of
76 $\delta^{18}\text{O}$ and $\delta^2\text{H}$ in liquid water samples when coupled to a CRDS analyzer. Here we present initial laboratory and
77 field verification experiments with this device, which we have combined with a dual-channel ion chromatograph



78 (IC; Metrohm AG, Herisau, Switzerland) for real-time analysis of major cations and anions. Laboratory
79 experiments quantifying the precision and sample carryover memory effects of this system are presented in
80 Section 3 below. Section 4 illustrates the practical application of the system in the field using a 28-day
81 deployment at a small catchment in Switzerland. Section 5 quantifies the fractions of event water that
82 contributed to the flood hydrograph in eight major precipitation events, illustrating one potential application of
83 high-frequency isotope tracer measurements.

84 2. Methodology

85 2.1 Isotope analysis and ion chromatography

86 For the analysis of the stable water isotopes ^{18}O and ^2H , the Continuous Water Sampler module (CWS; Picarro
87 Inc., Santa Clara, CA, USA) was coupled to a Wavelength Scanned-Cavity Ring-Down Spectrometer (WS-
88 CRDS; model L2130-*i*, Picarro Inc., Santa Clara, CA, USA). In the CWS, the water sample flows at a rate of
89 $\sim 1\text{ mL min}^{-1}$ through an expanded polytetrafluoroethylene (ePTFE) membrane tube. This tube is mounted in a
90 stainless steel chamber that is supplied with dry air to facilitate the steady diffusion of a small fraction of the
91 through-flowing water as vapor through the membrane. Through the continuous flow of dry air over the outer
92 surface of the membrane, the vapor is carried directly to the CRDS for isotope analysis. To minimize
93 temperature-induced fractionation effects, the instrument keeps the temperatures of the membrane chamber and
94 the inflowing water constant at (± 1 standard deviation) $45\pm 0.1^\circ\text{C}$ and $15\pm 0.1^\circ\text{C}$, respectively. A solenoid
95 diaphragm pump situated upstream of the membrane cartridge draws water samples from the sample container
96 and pushes them through the membrane tube at a flow rate of approximately 1 mL min^{-1} . As we show in
97 Section 3.1 below, preliminary tests showed that this pump is not sufficient for our purposes, so we substituted a
98 programmable high-precision dosing unit (800 Dosino, Metrohm AG, Herisau, Switzerland) in its place.
99 Isotopic abundances are reported through the δ notation relative to the VSMOW-SLAP standards. We used the
100 factory calibration of the isotope analysis system, because only relative isotope values are needed for
101 quantifying precision, drift, and carryover, and thus the absolute isotope values are unimportant.

102
103 Major ions in liquid water samples, i.e. Na^+ , K^+ , NH_4^+ , Ca^{2+} , Mg^{2+} , F^- , Cl^- , NO_3^- , SO_4^{2-} , PO_4^{3-} , were analyzed
104 with an ion chromatograph (IC; model 940 Professional IC Vario, Metrohm AG, Herisau, Switzerland) with a
105 two-column configuration (Anions: Metrosep A Supp 5 – 250/4.0, Cations: Metrosep c 6 – 250/4.0).
106 Continuous operation of the instrument was possible due to fully automated eluent generation (941 Eluent
107 Production Module). To generate the full ion chromatograms of both anions and cations, approximately 28min
108 were required; thus the sampling interval of the combined analysis system was fixed at 30min.

109 2.2 Sample collection and distribution

110 The water samples were distributed between the analyzers with high-precision dosing units (800 Dosino, here
111 called simply ‘Dosino’; Metrohm, Herisau, Switzerland). A Dosino contains a programmable piston that fills
112 and empties a glass cylinder with up to 50 mL of sample at a resolution of 10,000 increments (implying $5\ \mu\text{L}$
113 increment⁻¹). The design of the dosing unit minimizes the dead volume and thus the potential for sample



114 carryover. In the base of the glass cylinder sits a rotating valve disc that guides the liquid sample through one of
115 four ports; thus each Dosino functions as both a switching valve and a syringe pump.

116

117 Figure 1 depicts the schematic overview of the automatic sample collection and analysis system, showing how
118 the different Dosinos distribute precipitation and streamwater samples between the isotope analyzer, the IC and
119 and an autosampler (which can be programmed to save individual samples for subsequent analysis in the
120 laboratory). The sampling routine begins with a cleaning step when either the ‘P Dosino’ or the ‘S Dosino’
121 transports 10 mL of sample water for rinsing to the beaker. The ‘Isotope Dosinos’ also eject any remaining
122 sample into the beaker, after which the beaker is emptied. Then, 50 mL of fresh streamwater or precipitation
123 sample is transported (by either the ‘S Dosino’ or the ‘P Dosino’ for streamwater or precipitation, respectively)
124 into the rinsed beaker, from which one of the ‘Isotope Dosinos’ draws 30 mL of water and injects it at a flow
125 rate of 1 mL min⁻¹ into the CWS for isotope analysis. The two ‘Isotope Dosinos’ operate alternately to
126 minimize the time when the sample flow into the CWS is interrupted. Meanwhile, either the ‘P Dosino’ or the
127 ‘S Dosino’ takes up another 12 mL of water sample and pumps it through a 0.45 µm tangential filter into the ‘IC
128 Dosino’, which discards the first 2 mL of the filtered sample. From the remaining filtered sample, 8 mL are
129 filled into vials by the autosampler and 2 mL are delivered to the IC for direct ion analysis. During the ion
130 analysis (ca. 28 min), the ‘S Dosino’, ‘P Dosino’ and ‘IC Dosino’, the autosampler, and all tubing are rinsed
131 with nanopure water to minimize carryover effects. The entire sampling routine is programmed with the IC
132 control software MagIC Net (Metrohm, Herisau, Switzerland), which facilitates detailed data logging and
133 documentation of the sample handling.

134 3. Laboratory experiments

135 3.1 Optimization of sample injection into the Continuous Water Sampler module (CWS)

136 In the original design of the CWS, water samples are transported by a small solenoid diaphragm pump between
137 the inlet port and the membrane cartridge at a flow rate of approximately 1 mL min⁻¹. During preliminary tests,
138 however, we observed that raising or lowering the sample container detectably altered the reported isotope
139 ratios. In order to quantify the sensitivity of the instrument to hydraulic head differences (i.e., the height of the
140 water table in the sample bottle relative to the waste outlet of the CWS), we changed the elevations of the
141 sample container relative to instrument while continuously analyzing a single water sample (nanopure water).
142 We measured vapor concentration, $\delta^{18}\text{O}$ and $\delta^2\text{H}$ for the same water sample at five different elevations, ranging
143 from 7 cm above to 98 cm below the waste outlet. The end of the waste outlet tube was always freely draining.
144 Each configuration was measured for one hour and the average values and standard deviations of the
145 uncalibrated 6s measurements of vapor concentration, $\delta^{18}\text{O}$ and $\delta^2\text{H}$ were calculated from the last 10min of each
146 1h configuration.

147

148 The results of this experiment are summarized in Fig. 2, which shows clear linear relationships between the
149 hydraulic head differences and both the vapor concentrations and the isotope measurements. Lowering the
150 sample source relative to the outflow results in systematically heavier isotopic values in the vapor measured by
151 the instrument. Vapor concentrations show a similar trend, i.e. more vapor was generated for lower positions of



152 the sample source. These observations suggest that the hydraulic head difference directly affected the flow rate
153 of the liquid sample through the CWS membrane tube. Because the water is much colder than the surrounding
154 air as it enters the membrane chamber, it is continuously warming as it travels through the membrane tube. At
155 greater head gradients (and thus smaller flow rates), the sample will travel more slowly through the membrane
156 chamber and will warm up more. As a consequence of higher water temperatures, water can be expected to
157 diffuse more rapidly through the membrane and the resulting vapor can be expected to be less fractionated
158 relative to the liquid phase (Kendall and McDonnell, 1998), as observed in Fig. 2.

159

160 It is unknown whether the empirical linear relationships shown in Fig. 2 are generally applicable, or are specific
161 to each individual membrane or to the properties of the sample. Nevertheless, for this membrane and this
162 sample, the results indicate that changing the hydraulic head by 50 cm changes the reported isotope values by
163 approximately 0.12 ‰ for $\delta^{18}\text{O}$ and 0.52 ‰ for $\delta^2\text{H}$, respectively. This flow-rate artifact might become
164 particularly important for applications in which isotope standards and samples are drawn from sample
165 containers at different elevations relative to the waste outlet of the CWS (e.g. shipboard sampling). In such
166 cases, a vapor concentration correction relative to a reference height would have to be carried out to account for
167 the changes in flow rate that affects the isotopic composition in the measured water vapor. Alternatively, a
168 different injection system could be used to deliver a specified flow rate, independent of the position of the
169 source relative to the CWS. We used the Dosino for this purpose, since it functions as a high-precision syringe
170 pump whose delivery rate is specified by the pulse rate of the stepper motor, independent of the hydraulic head
171 gradient.

172

173 Because of the limited volume of each Dosino's glass cylinder (50 mL), a sample could be injected at a flow
174 rate of 1 mL min^{-1} for a maximum of 50min. For longer injections, or to switch samples, a second Dosino had
175 to take over the sample delivery. The handoff between the Dosinos interrupted the sample flow to the CWS for
176 around 2s. This interruption was reflected in a sharp but brief increase in vapor concentrations and isotope
177 values, which returned back to stable values approximately 10min after the injection started (see Fig. 3 for an
178 example). For our application, i.e. synchronous IC measurements, we programmed a 30min injection period for
179 the isotope analysis. To obtain the final isotope values of a liquid sample we averaged the individual 6s
180 measurements reported by the WS-CRDS during the last 10min of each 30min injection period, using the first
181 20min to minimize any memory effects from the previous sample or from Dosino changeover. The advantage
182 of the Dosino-based sample injection is the very steady, pressure-independent sample injection.

183 **3.2 Performance of the isotope analyzer with Continuous Water Sampler (CWS)**

184 We quantified precision, drift coefficients and carryover effects of the isotope analyzer with CWS and Dosino-
185 based sample injection, using a continuous 48h laboratory experiment that alternated between three water
186 samples (i.e., to mimic streamwater, precipitation and a reference standard). The sample handling system was
187 as shown in Fig. 1, except that the precipitation collector was replaced with a 10 L bottle of nanopure water and
188 the streamwater sampler was replaced by a 10 L bottle of tap water. The sampling system alternated between
189 these two sources, and for each eighth injection it introduced an isotopically heavier secondary standard (Fiji
190 bottled water) (Fig. 3). The isotopic differences between Fiji bottled water and tap water were about



191 (± 1 standard error, SE) 4.54 ± 0.02 ‰ and 32.67 ± 0.08 ‰ for $\delta^{18}\text{O}$ and $\delta^2\text{H}$, respectively. The isotopic
 192 differences between tap water and nanopure water were much smaller (0.05 ± 0.01 ‰ for $\delta^{18}\text{O}$ and
 193 0.12 ± 0.03 ‰ for $\delta^2\text{H}$) because the nanopure water was generated from the same tap water by reverse osmosis.
 194

195 The precisions of the isotope values, as quantified by the standard deviations of the individual 6s measurements
 196 during the last 10min of each injection period, were better than 0.08 ‰ for $\delta^{18}\text{O}$ and 0.18 ‰ for $\delta^2\text{H}$. These
 197 standard deviations imply that the standard errors of the 10min averages should be better than 0.008 ‰ and
 198 0.018 ‰ for $\delta^{18}\text{O}$ and $\delta^2\text{H}$, respectively. These standard errors overestimate the repeatability of successive
 199 measurements, however. As a measure of sample-to-sample repeatability, the standard deviations of the 10min
 200 averages for the entire 48h experiment were 0.03 ‰ ($\delta^{18}\text{O}$) and 0.17 ‰ ($\delta^2\text{H}$), or better, for each of the three
 201 water samples (excluding two outliers associated with an interruption in the sampling routine), much larger than
 202 the calculated standard errors. Thus, the major uncertainties in the 10min averages do not arise from the
 203 counting statistics of the instrument itself, but rather, we suspect, from sample-to-sample variability in the
 204 performance of the vaporizer. We use these larger estimates of uncertainty (0.03 ‰ for $\delta^{18}\text{O}$ and 0.17 ‰ for
 205 $\delta^2\text{H}$) in the error propagation calculations presented in Section 5.1.
 206

207 Instrument drift was analyzed by linear regression of the 10min averages from the ends of each 30min injection
 208 period. Instrument drift for $\delta^{18}\text{O}$ was statistically indistinguishable from zero for two of the three waters,
 209 averaging ($\pm 1SE$) -0.009 ± 0.008 , -0.009 ± 0.006 , and -0.015 ± 0.007 ‰ day^{-1} for Fiji, nanopure, and tap water,
 210 respectively. Instrument drift for $\delta^2\text{H}$ was slow but statistically significant for two of the three waters, averaging
 211 0.133 ± 0.040 , 0.084 ± 0.016 , and -0.021 ± 0.021 ‰ day^{-1} for Fiji, nanopure, and tap water, respectively. Thus the
 212 accumulated drift over one day was typically smaller than the measurement precision for individual 10min
 213 averages for either isotope. As explained in Section 4.2 below, substantially faster drift occurred during the
 214 field experiment due to biofilm growth on the membrane, but could be easily measured and corrected using
 215 regularly injected reference standards.
 216

217 Between-sample memory mainly arises from small remnants of previously injected samples that remain in the
 218 sample handling system (e.g., tubes, membrane, valves, pumps) or the analyzer itself, and are carried over to the
 219 following analysis. We quantified the between-sample memory effect of the isotope analyzer using two
 220 isotopically contrasting samples, Fiji water and nanopure water. The true isotopic difference was obtained from
 221 the 7th (=last) injection of nanopure water, which was measured around 3h after the reference standard (Fiji),
 222 and was thus assumed to be free of any memory effects. We calculated the memory coefficient (X) as a measure
 223 of carryover effects using Gupta et al. (2009):

$$224 \quad X = \frac{C_i - C_{i-1}}{C_{true} - C_{i-1}} \quad (1)$$

225 where C denotes the isotope ratio (or the solute concentration), the indices (i) and ($i-1$) denote the current and
 226 the previous injection, and ($true$) denotes the true value taken from the last value of multiple injections. The
 227 average carryover from the Fiji bottled water to the next 30min sample was $100\% \cdot (1-X) \approx 0.9\%$ for $\delta^{18}\text{O}$ and
 228 1.2% for $\delta^2\text{H}$, respectively (Table 1).



229 **3.3 Performance of the ion chromatograph (IC)**

230 With the IC, a 48h laboratory experiment was carried out as well. However, the sampling sequence differed
231 slightly from that of the isotope analyzer described previously: each measurement of tap water or Fiji water was
232 followed by two to six samples of nanopure water, which mimics precipitation samples with generally very low
233 solute concentrations. Due to the low solute concentrations in the nanopure water, carryover effects can be
234 quantified efficiently.

235

236 Average concentrations, of the major anions and cations during the 48h experiment are reported in Table 1,
237 along with their absolute and relative standard deviations. For tap water and Fiji water, relative standard
238 deviations were <5% for all constituents with concentrations above the limit of quantification (LOQ), indicating
239 that the IC measurements were stable over the 48h period. Consequently, drift effects in the instrument were
240 not statistically significant ($p>0.05$) for most constituents in Fiji water and tap water. For Cl^- , NO_3^- and SO_4^{2-} in
241 the Fiji water, the linear drift was statistically significant but also very slow: accumulated drift over 24h was
242 never much larger than the LOQ (Table 1). Average % carryover ($100\% \cdot (1-X)$, Eq. (1)) in the nanopure water
243 sample, following immediately after a tap water or Fiji water sample, was $\leq 3.8\%$.

244 **4. Application in the field**

245 **4.1 Setup**

246 For the field experiment, the system was installed in a hut next to a small perennial stream flowing behind the
247 Swiss Federal Institute for Forest, Snow and Landscape Research (WSL) near Zurich, Switzerland. The creek
248 drains an area mainly covered with open grassland, grain fields, and suburban residential neighbourhoods (Fig.
249 4). The dominant soil type is colluvial, partly gleyic brown soil (GIS-ZH, 2016).

250

251 Stream stage, temperature and electrical conductivity were recorded in the stream every 10min using a data-
252 logging sonde (model DL/N 70; STS SensorTechnik Sirmach, Switzerland). The volumetric discharge was not
253 gauged, but we assume that the times of the highest stream stage coincided with peak flow, and thus use both
254 terms synonymously. Precipitation (rainfall and snow) was measured with an unheated collector daily at
255 7:30am. For a higher temporal resolution, precipitation rates at the site were estimated as the average of 10min
256 measurements at three nearby weather stations (Stetten, Zurich Fluntern, and Zurich Affoltern) in the
257 MeteoSwiss observation network. Good agreement ($R^2 > 0.82$) was observed between measured daily
258 precipitation at our field site and the daily sums of the averages of the three MeteoSwiss stations, thus indicating
259 that the MeteoSwiss data are a reasonable proxy for precipitation rates at the field site. To distinguish rain and
260 snowfall events, air temperature was recorded near the instrument hut every 10min (Haeni, 2016; Schaub et al.,
261 2011).

262

263 A submersible pump (Eheim GmbH, Deizisau, Germany) continuously pumped streamwater at a rate of
264 6 L min^{-1} into a through-flow bucket inside the hut. The volume of the bucket was 10 L; thus every several
265 minutes the contents of the bucket were effectively exchanged. Every 30min, water was drawn from the bucket
266 by the 'S Dosino' through a $1\mu\text{m}$ cellulose filter to supply the isotope analyzer, IC and autosampler (Fig. 1).



267 Precipitation was collected with a heated 45cm diameter funnel installed 2.5m above ground. Precipitation
268 flowed into a Teflon®-coated collector with a level detector that triggered at a threshold volume of 72 mL
269 (equating roughly 0.5 mm of precipitation). The status of the level detector was queried before the end of each
270 measurement routine and a precipitation sample was drawn only if the threshold volume was exceeded. For
271 initial filtration of the precipitation sample, a ceramic frit filter was attached on the suction tube of the ‘P
272 Dosino’ that drew the sample from the precipitation collector. After precipitation was sampled, a peristaltic
273 pump emptied the precipitation collector to avoid mixing fresh and old precipitation samples. The sampling
274 routine was programmed to always alternate between streamwater and precipitation samples in order to obtain
275 enough streamwater samples during storm periods. To reduce biofilm growth on the membrane in the CWS,
276 copper wool was placed in the beaker from which the ‘Isotope Dosinos’ drew the samples. Sampling was
277 interrupted approximately once a week for basic maintenance (i.e., replacing the filter membranes, cleaning
278 Dosinos, refilling reference standards and eluent stock solutions).

279
280 Reference standards were analyzed every 3h to correct for instrument drift. Correction for drift was carried out
281 for the five samples between two bracketing measurements of the same reference standard:

$$282 \quad C_{corr} = C_{raw} + (C_{true} - \frac{C_{std,i} + C_{std,j}}{2}) \quad (2)$$

283 with C denoting the solute concentration or the isotope ratio, respectively. The indices represent the corrected
284 value ($corr$), the current raw measurement (raw), the true value of the reference standard ($true$), and the
285 previous and successive measurements of the same reference standard (std) measured at time i and 3h later at
286 time j . For the isotope analyzer, Fiji bottled water was used as drift control, which was injected directly by one
287 of the ‘Isotope Dosinos’ (Fig. 1). The measurements of the IC were drift-corrected with another reference
288 standard (Evian bottled water) in the autosampler transferred directly to the IC by the ‘IC Dosino’. Evian
289 bottled water was used as its mineral composition resembles that of streamwater more closely than Fiji bottled
290 water.

291 **4.2 Temporal high-resolution measurements of stable isotopes and major ions in precipitation and** 292 **streamwater**

293 The measurement system was deployed at the field site from 13 February 2016 to 11 March 2016 and more than
294 1000 streamwater and precipitation samples were analyzed for stable water isotopes and major ions. Although
295 the field-based measurement period covered only around 1 month, this real-time analysis system captured a
296 wide range of hydrological and hydrochemical conditions. Table 2 provides an overview of the eight storm
297 events during that period. A comparison of the aggregated precipitation data with the on-site daily
298 measurements from the un-heated rainfall collector indicated that precipitation during Events #1-#7 was mostly
299 rainfall. Snowfall occurred occasionally after 1 March, while during Event #8 most precipitation fell as snow.

300
301 We calculated the response time of streamflow as the time difference between the first detection of precipitation
302 and the first significant increase in streamwater level relative to the initial conditions. Typical response times
303 were between 0h and 2h (Table 2), suggesting an influence from the residential area in the eastern part of the
304 catchment. A more delayed streamflow response (4h) was observed after the snowfall event (#8), reflecting
305 delayed snowmelt. As illustrated by Fig. 5, a 30min sampling interval was sufficient to resolve the temporal



306 patterns of stable isotopes and solutes in streamflow during the rising limb of the hydrograph, even during low-
307 intensity precipitation periods such as Event #5.

308

309 Compared to the laboratory experiment with the isotope analyzer, during the field experiment we observed
310 carryover effects in the isotope measurements of up to $100\% \cdot (1-X) = 3\%$, which can be explained by the copper
311 wool in the beaker from which the “Isotope Dosinos” drew the water samples. Despite the rinsing routine of the
312 beaker, the wool retained small volumes of sample from previous injections that affected the isotopic
313 composition in the fresh sample. Consequently, the wool was removed and the prior isotope measurements
314 were adjusted with $X=97\%$ and Eq. (1). Further, instrument drift was substantially faster during the beginning
315 of the field experiment due to biofilm growth in the membrane tube. For instance, during the first week,
316 instrument drift for raw $\delta^{18}\text{O}$ and $\delta^2\text{H}$ measurements in Fiji bottled water was statistically significant, averaging
317 ($\pm 1SE$) -0.185 ± 0.006 and $-0.288 \pm 0.015 \text{ ‰ day}^{-1}$, respectively.

318

319 Figure 6a depicts the local meteoric water line obtained from the isotopic measurements in precipitation. The
320 isotopic composition of precipitation varied over a range of 14.9 ‰ in $\delta^{18}\text{O}$ and 109.4 ‰ in $\delta^2\text{H}$. A correlation
321 between air temperature and the isotopic composition of precipitation is evident during most storm events.

322 Figure 5 shows that, for instance, precipitation samples became isotopically heavier during Events #2 and #8
323 when air temperature increased, while the opposite behavior was observed during Events #1, #3 and #5, when
324 air temperature decreased. During Events #4, #6 and #7, however, the correlation with temperature was not as
325 distinct as during the other five events.

326

327 The isotopic composition of streamwater varied by less than half as much as that of precipitation, i.e. by 5.9 ‰
328 for $\delta^{18}\text{O}$ and by 43.6 ‰ for $\delta^2\text{H}$, respectively (Fig. 6b). For all eight events, the isotopic signature of pre-event
329 streamwater was relatively constant, averaging $-10.89 \pm 0.21 \text{ ‰}$ for $\delta^{18}\text{O}$ and $-74.88 \pm 1.40 \text{ ‰}$ for $\delta^2\text{H}$,
330 respectively (± 1 standard deviation, $n=8$). During the events, $\delta^{18}\text{O}$ and $\delta^2\text{H}$ in streamwater changed by up to
331 4.54 ‰ and 34.43 ‰ , respectively (Event #7).

332

333 For the IC, memory effects were negligible during the field experiment (because the sample did not make
334 contact with the copper wool), so the measurements were corrected only for drift effects. Solute concentrations
335 in precipitation and streamwater varied widely, as shown for instance in Fig. 5 for Cl^- and NO_3^- . For Li^+ , NH_4^+ ,
336 K^+ , F^- and PO_4^{3-} in streamwater, as well as concentrations of Mg^{2+} in precipitation, measured concentrations
337 were generally below the LOQ. NO_3^- (as well as Ca^{2+} and SO_4^{2-} , not shown) in streamwater exhibited clear
338 dilution patterns during all precipitation events (Fig. 5d). Concentrations of NO_3^- , Ca^{2+} and SO_4^{2-} in
339 precipitation during the eight events were on average (± 1 standard deviation) $1.5 \pm 1.1 \text{ mg L}^{-1}$, $12.1 \pm 2.9 \text{ mg L}^{-1}$
340 and $0.5 \pm 0.8 \text{ mg L}^{-1}$, respectively. Solute concentrations in pre-event streamwater were on the order of (± 1
341 standard deviation) $11.7 \pm 1.8 \text{ mg L}^{-1}$ for NO_3^- , $160.8 \pm 9.7 \text{ mg L}^{-1}$ for Ca^{2+} and $21.5 \pm 3.3 \text{ mg L}^{-1}$ for SO_4^{2-} , whereas
342 concentrations during all events dropped to values as low as 3.73 mg L^{-1} (NO_3^-), 64.6 mg L^{-1} (Ca^{2+}) and
343 5.12 mg L^{-1} (SO_4^{2-}). In contrast, the concentrations of Cl^- (and Na^+ , not shown) in streamwater showed dilution
344 patterns until Event #3, and then showed distinct enrichment patterns occurred thereafter (Fig. 5c), likely



345 associated with road salt wash-off. Due to possible road-salt effects on Na^+ and Cl^- , we will focus on Ca^{2+} , NO_3^-
346 and SO_4^{2-} in the analysis below.

347 5. Comparison of event-water fractions estimated from isotopes and chemical tracers

348 5.1 Hydrograph separation and uncertainty analysis

349 To illustrate a potential application of high-frequency isotope and chemical measurements, here we quantify the
350 event-water fractions during the eight major events captured during the 1-month observation period. We used
351 two-component end-member mixing analysis to quantify the fractions of event water in streamflow during the
352 precipitation events. We applied the conventional mass balance equation (Pinder and Jones, 1969):

$$353 F_E = \frac{Q_E}{Q_S} = \frac{C_S - C_P}{C_E - C_P} \quad (3)$$

354 The fraction of event water relative to total streamflow ($F_E = Q_E/Q_S$) was calculated from the isotope values or
355 solute concentrations in total streamflow (C_S), event precipitation (C_E) and pre-event streamflow (C_P). Here, C_P
356 was obtained for each event from the average of the five streamwater samples immediately before the onset of
357 precipitation. The value of C_E was the incremental, volume-weighted mean (McDonnell et al., 1990) of all
358 precipitation samples that were collected before the respective streamflow sample:

$$359 C_{E,j} = \frac{\sum_{i=k}^j P_i C_i}{\sum_{i=k}^j P_i} \quad (4)$$

360 with P_i being the precipitation depth associated with the isotope value (or solute concentration) C_i collected at
361 time i since the starting time k of the precipitation event.

362 Uncertainty in the hydrograph separation was quantified with Gaussian error propagation (Genereux, 1998),
363 using calculated standard errors (SE) arising from analytical uncertainties and the temporal variability of the
364 isotope values (or solute concentrations). Because C_E is a volume-weighted mean, the standard error SE_{C_E} is
365 calculated with

$$366 SE_{C_{E,j}} = \left[\frac{\sum_{i=k}^j P_i (C_i - C_{E,j})^2}{(j-k) \sum_{i=k}^j P_i} \right]^{1/2} \quad (5)$$

367 where $C_{E,j}$ denotes the volume-weighted mean, C_i denotes the i^{th} concentration that comprises that mean, and (j)
368 is the number of samples included in the volume-weighted mean. The standard error of C_S , SE_{C_S} , arises from
369 the measurement uncertainties given in Table 1. For SE_{C_P} , the same measurement uncertainties are applied, as
370 well as the temporal variability of the five measurements comprising C_P . The standard error of the event-water
371 fraction (SE_{F_E}) can then be obtained by Gaussian error propagation:

$$372 SE_{F_E} = \left\{ \left[\frac{-1}{C_P - C_E} SE_{C_S} \right]^2 + \left[\frac{C_S - C_E}{(C_P - C_E)^2} SE_{C_P} \right]^2 + \left[\frac{C_P - C_S}{(C_P - C_E)^2} SE_{C_E} \right]^2 \right\}^{1/2} \quad (6)$$

373

374 5.2 Event-water fractions for eight storm events

375 The varied weather conditions during the 28-day field experiment led to complex hydrologic responses,
376 resulting in a data set that illustrates the potential of these high-frequency measurements for hydro-chemical
377 analyses. Mixing analysis for two end-members, event water and pre-event water, was carried out for eight
378 storm events between 20 February and 8 March 2016, based on isotopic and chemical tracers. Event #8, where



379 precipitation fell partly as snow, was included in the analysis as river discharge and streamwater EC responded
380 within 4h after the onset of precipitation (Table 2). Hence, the temporal change in the snowmelt isotopic signal
381 due to fractionation was assumed to be negligible.
382

383 Isotope hydrograph separation (IHS) was performed using both $\delta^{18}\text{O}$ and $\delta^2\text{H}$, whereas chemical hydrograph
384 separation (CHS) was carried out with the three constituents Ca^{2+} , NO_3^- and SO_4^{2-} (Cl^- and Na^+ , were not used
385 for CHS due to the influence of road salt at the site). We also performed hydrograph separation based on
386 streamwater EC, since several studies have used EC in lieu of chemical concentrations for hydrograph
387 separation, owing to the ease of obtaining continuous EC measurements (e.g., Dzikowski and Jobard, 2012;
388 Matsubayashi et al., 1993; Muñoz-Villers and McDonnell, 2012; Pellerin et al., 2008). As we did not measure
389 EC in precipitation directly, we had to estimate it empirically. For this, we used a standard conversion equation,
390 i.e., the pseudo-linear approach following Sposito (2008), to calculate EC in precipitation from the ionic
391 strength of the major cations and anions in the precipitation samples. We assume that the ion concentrations
392 measured by the IC account for the great majority of the ionic strength. In order to estimate the uncertainty of
393 this method, we also calculated the EC values in streamwater and compared them with the actual measurements
394 of the EC probe in the stream. The (absolute value) difference between the calculated and measured
395 streamwater-EC values averaged $20 \mu\text{S cm}^{-1}$.
396

397 For the uncertainty analysis of the calculated event-water fractions, analytical uncertainties of the isotope
398 measurements were assumed to be 0.03 ‰ and 0.17 ‰ for $\delta^{18}\text{O}$ and $\delta^2\text{H}$, respectively (Section 3.2, Table 1).
399 Relative uncertainties of the IC measurements were $0.006 \cdot C + 0.087 \text{ mg L}^{-1}$ for Ca^{2+} , $0.028 \cdot C + 0.002 \text{ mg L}^{-1}$ for
400 NO_3^- and $0.037 \cdot C + 0.006 \text{ mg L}^{-1}$ for SO_4^{2-} , respectively ((where C is concentration in mg L^{-1} ; Table 1). For the
401 EC values, a measurement uncertainty of 2% was assumed for the EC probe based on the specifications given
402 by the EC probe's manufacturer. The assumed uncertainty in the EC values in precipitation was $20 \mu\text{S cm}^{-1}$, as
403 calculated above.
404

405 Two illustrative precipitation events, together with their hydrologic, isotopic and chemical responses in
406 streamwater, are shown in Figs. 7 and 8 (Events #1 and #2, respectively). During Event #1, total rainfall was
407 6.7 mm within 10h 40min, while 10.3 mm rain fell within 9h 40min during Event #2. Antecedent moisture
408 conditions, estimated by the total rainfall within 48 h and 24 h before the event, as well as initial streamwater
409 level, were relatively wet for Event #1 and relatively dry for Event #2 (Table 2).
410

411 For Event #1, $\delta^{18}\text{O}$ and $\delta^2\text{H}$ in streamwater followed the observed patterns in precipitation, i.e. streamwater
412 became isotopically lighter over time. Isotope hydrograph separations for this event yield maximum event-
413 water fractions ($F_{E,\text{max}}$) of $78 \pm 10 \%$ and $60 \pm 14 \%$ for $\delta^{18}\text{O}$ and $\delta^2\text{H}$, respectively, similar to the results obtained
414 from the chemical tracers Ca^{2+} , NO_3^- and SO_4^{2-} ($57 \pm 1 \%$, $65 \pm 2 \%$ and $65 \pm 3 \%$) and EC ($56 \pm 3 \%$, Fig. 7d and e).
415 The fraction of event water increased rapidly after the start of rainfall and declined continuously as stream stage
416 receded. A difference in response timing is evident for the chemical and isotope tracers in Fig. 7d and 7e: The
417 chemical tracers exhibited the strongest dilution effect during peak flow, whereas the isotope tracers showed the
418 largest response to the event roughly 2h later, possibly because the isotopic signature in precipitation became



419 lighter as the event progressed. Consequently, if C_S at the time of Q_{\max} were used to perform hydrograph
420 separation (Eq. (3)), isotope-based F_E -values would be substantially smaller (i.e., $43\pm 6\%$ and $42\pm 9\%$ for $\delta^{18}\text{O}$
421 and $\delta^2\text{H}$, respectively) than the $F_{E,\max}$ -values reported above.

422

423 During Event #2, the solutes in streamwater showed a clear dilution signal (Fig. 8c), similar to Event #1. The
424 isotopic composition in streamwater, by contrast, showed only a very weak and inconsistent response to
425 precipitation. For instance, $\delta^2\text{H}$ in precipitation increased continuously through the event, whereas $\delta^2\text{H}$ in
426 streamwater first decreased and then, ca. 4 h after the onset of precipitation, began to increase again.
427 Consequently, IHS and CHS yield substantially different interpretations for Event #2. Maximum event-water
428 fractions based on CHS ranged from $68\pm 1\%$ (Ca^{2+}) to $83\pm 5\%$ (NO_3^-), similar to Event #1. In contrast, $F_{E,\max}$ -
429 values based on IHS ranged from $7\pm 1\%$ to $16\pm 3\%$, indicating that pre-event water was the dominant source of
430 streamwater during peak flow.

431

432 How can such a large discrepancy between the event-water fractions calculated from different environmental
433 tracers be explained? From Fig. 5 it can be seen that precipitation was isotopically lighter than streamwater
434 during the six days leading up to Event #2. Thus, the initial decrease in the $\delta^{18}\text{O}$ and $\delta^2\text{H}$ values in streamwater
435 during Event #2 suggests the release of isotopically lighter soilwater and groundwater that were recharged
436 during previous events. An activation of this pre-event water storage might have been triggered by enhanced
437 infiltration after relatively dry antecedent moisture conditions (AMC), compared to the previous event, whereas
438 wet AMC would be more consistent with surface runoff generation. This hypothesis is further supported by the
439 isotopic responses in streamwater during Event #5, another isotopically heavy event with dry AMC, following
440 earlier inputs of isotopically lighter precipitation. In Event #5, small event-water fractions ($12\pm 1\%$ and $20\pm 1\%$
441 for $\delta^{18}\text{O}$ and $\delta^2\text{H}$, respectively; Fig. S1) were again obtained, indicating that pre-event water dominated
442 streamflow, similarly to Event #2. And in Event #5, just as in Event #2, the chemical tracers showed strong
443 dilution, leading to an overestimate of the event-water fraction ($>40\pm 2\%$). In both Event #2 and Event #5, the
444 chemical and isotopic data point to a large contribution from recent antecedent moisture that had not yet become
445 highly mineralized, rather than from either event precipitation or from older groundwater that presumably
446 accounted for most of the pre-event baseflow.

447

448 Figure 9 summarizes the estimated event-water fractions for all eight events, based on IHS and CHS, for two
449 points in time during each event: the time with the largest isotopic or chemical response (i.e., $F_{E,\max}$) and the
450 time of peak flow (Q_{\max}). Maximum event-water fractions varied greatly across the eight events (for example,
451 from $16\pm 3\%$ to $68\pm 14\%$ based on $\delta^2\text{H}$, Fig. 9, Table S1 and S2). Also, within individual events, hydrograph
452 separations based on different isotopic and chemical tracers differed, often by much more than their
453 uncertainties. Inconsistencies between the estimated event-water fractions can be explained with the fact that
454 different tracers are shaped by different hydrochemical processes and flow pathways, and thus may describe
455 different end-members (e.g., Richey et al., 1998; Wels et al., 1991). While stable water isotopes are considered
456 to be ideal conservative tracers, chemical tracers are altered by biogeochemical processes on their way through a
457 hydrological system. These biogeochemical processes also vary over time, as they depend on antecedent
458 conditions and precipitation characteristics. Continuous high-frequency analysis of environmental tracers can



459 document this temporal variability, which, in turn, helps to constrain conceptual catchment models. As
460 illustrated by Events #2 and #5, comparing chemical and isotopic tracers can be useful in identifying the
461 temporally variable contributions of different water storages in the subsurface.

462
463 Figure 9 illustrates further that for three events (#2, #5 and #8), estimated event-water fractions for the two
464 isotopes, $\delta^{18}\text{O}$ and $\delta^2\text{H}$, differed significantly (i.e., by more than twice their pooled uncertainties). These
465 differences did not follow any particular pattern, for instance, $F_E(\delta^{18}\text{O}) > F_E(\delta^2\text{H})$ for Event #8, while $F_E(\delta^{18}\text{O})$
466 $< F_E(\delta^2\text{H})$ for Events #2 and #5. A possible explanation for such discrepancies is that the isotopic signature of
467 precipitation sampled at one location might not be representative of the spatially distributed precipitation that
468 generated the sampled streamflow (e.g., Fischer et al., 2015; Lyon et al., 2009). Alternatively, the pre-event
469 streamflow signature (C_p) may not reflect the isotopic signature of the entire pre-event water storage, but only of
470 the components that feed baseflow (e.g., Klaus and McDonnell, 2013). Another way of viewing this problem is
471 that the precipitation event may have mobilized a third pre-event water storage with unknown isotopic
472 composition (e.g., Tetzlaff et al., 2014). This conjecture is strongly supported by the initial shift toward
473 isotopically lighter streamflow early in Event #2, even though the event precipitation was isotopically heavier
474 than the pre-event baseflow. Event #5 also shows divergent event-water fractions between the two isotopes, and
475 like Event #2, it also had strongly contrasting pre-event precipitation inputs. Thus, the history of both events
476 suggests that pre-event storage in this catchment was isotopically heterogeneous. This observation is
477 unsurprising, given the pervasive heterogeneity of typical catchments, but a more detailed explanation is not
478 possible with our spatially limited data set. Spatially distributed measurements, such as from groundwater and
479 soil water storages, would help in constraining the individual end-members that contribute to streamflow (e.g.,
480 Hangen et al., 2001). Additional high-frequency time series of the groundwater table and soil moisture profiles
481 would allow for documenting the effects of antecedent wetness conditions on the response times and on the
482 activation of different storages at the site. Finally, a spatially distributed precipitation sampling network might
483 help to fully quantify the uncertainty inherent in the event-water signature.

484 5.3 Variable response times of chemical and isotope tracers

485 Measuring isotopes and solutes at high temporal resolution over several storm periods allows for a detailed
486 investigation of response times of hydrological and hydrochemical variables and their linkages to the event
487 characteristics. As can be seen for instance in Fig. 7, during Event #1 the timing of the largest hydrological and
488 hydrochemical responses did not always coincide. For only three events (i.e., #2, #4, #6) the timing of peak
489 flow coincided with the $F_{E,\max}$ values for both chemical and isotope tracers. During Event #3, the isotope
490 tracers resulted in $F_{E,\max}$ values 1.5h±1.0 h before peak flow. For Events #7 and #8, which were affected by
491 snowmelt, both tracer types showed the strongest responses up to 2.0±1.0 h earlier than the actual flow peak. In
492 contrast, during Event #1 the peak responses in the isotope tracers and EC came up to 2.0h±1.0 h after peak
493 flow.

494
495 These examples illustrate that the hydrological conditions of the stream (i.e., the stream stage or flow rate) are
496 not reliable proxies for the timing of the maximum event-water contribution. As a consequence, collecting
497 samples only during or after peak flow may result in a significant underestimation of event-water fractions. Our



498 data indicate that the time window for sample collection at our site must extend more than 3h before and after
499 peak flow in order to capture the whole range of event water dynamics. In the case of the snowmelt Event #8,
500 the EC data suggest an even longer sampling period in order to capture unusual events such as the inflow of
501 water contaminated by road salt.

502

503 **5.4 The role of the sampling frequency for capturing hydrological and hydrochemical catchment** 504 **processes**

505 A sampling frequency can be considered optimal when the gain of information from additional measurements is
506 marginal (Kirchner et al., 2004; Neal et al., 2012). With our high-resolution data set we can thus investigate the
507 potential of different sampling frequencies for capturing hydrological and hydrochemical catchment processes,
508 by subsampling the time series at smaller sampling frequencies, i.e. at 3-hourly, 6-hourly, 12-hourly and daily
509 intervals. For concentrations and isotope values in streamwater, data were simply sub-sampled from the 30min
510 resolution time series to mimic grab sampling. To mimic the effects of integrated bulk precipitation samples,
511 concentrations in precipitation were calculated from the volume-weighted averages of the 30min data over the
512 respective time interval.

513

514 Figure 10 shows that 3h sampling intervals would still be sufficient to capture the isotopic variations in
515 streamwater, including during low-intensity precipitation events. However, the short-term variability within
516 single storm periods cannot be resolved at this lower sampling frequency. Thus, even sampling intervals of 3h
517 can result in a significant loss of information relative to 30min sampling, and at sampling intervals of 12h or
518 longer, diurnal fluctuations and some isotopic and chemical responses to low-intensity precipitation events
519 would also be lost. Likewise, the 6h or 12h bulk precipitation samples shown in Fig. 10 fail to reflect the large
520 isotopic variability revealed by the 30min samples.

521

522 To further illustrate the effect of lower sampling frequencies, we performed hydrograph separation with the
523 subsampled data sets, for which illustrative results are shown for the isotope tracer $\delta^2\text{H}$ in Fig. 11. With a
524 sampling interval of 3h, event-water fractions similar to those for the 30min sampling can still be obtained,
525 except for Event #3, when the 3h sampling interval captured a streamwater sample that was isotopically very
526 similar to the pre-event water. For Events #2, #3, #5 and #7, longer sampling intervals underestimate event-
527 water fractions. With 12h sampling intervals, IHS with $\delta^2\text{H}$ yields much smaller event-water fractions for all
528 events except Event #4, and yields unrealistic results for two Events (#1, #5), as the isotopic differences
529 between the two end-members become too small.

530

531 Because the hydrologic response times in this catchment were mostly much shorter than 2h, the durations of the
532 maximum hydrochemical variations were similarly short. Thus, sampling at longer time intervals increases the
533 risk of missing this critical peak response; if the sample is taken before or after the maximum hydrochemical
534 response, the event-water signal in streamwater (C_s) may be too weak, which will inevitably underestimate
535 event-water fractions, or even lead to unrealistic negative values.



536 **6 Concluding remarks**

537 This paper presents the first field hydrology application of Picarro's Continuous Water Sampler (CWS) module,
538 which was coupled to a L2130-*i* Wavelength Scanned-Cavity ring-down Spectrometer to measure the stable
539 water isotopes $\delta^{18}\text{O}$ and $\delta^2\text{H}$ in streamwater and precipitation at a temporal resolution of 30min. We combined
540 this real-time isotope analysis system with a dual-channel ion chromatograph for synchronous analysis of major
541 cations and anions. Good instrument performance and high measurement precision could be achieved during
542 continuous 48h laboratory experiments and a 28-day deployment in the field at a small, partly urbanized
543 catchment in central Switzerland.

544

545 Problematic issues such as sample degradation during storage and transportation, which arise in conventional
546 sampling for catchment tracer studies, become irrelevant with the system presented here. At the same time,
547 potential registration errors arising during the collection and handling of large numbers of water samples are
548 avoided. Conversely, two major limitations of the coupled isotope analyser / IC system are its high cost, and the
549 need for sufficient electrical power (around 1.7 kW), constraining its use in remote locations. However,
550 laboratory analysis of conventionally collected grab samples is also cost-intensive, and autosamplers used in
551 conventional sampling schemes also require a reliable energy supply (though at much lower power levels).

552

553 The results of the high-frequency analysis system were presented here to provide a proof-of-concept and an
554 illustration of its functionality at the field, rather than to fully document the hydrological and biogeochemical
555 processes at this field site. A more detailed interpretation would require additional measurements of soilwater
556 and groundwater isotopes and chemistry, in order to better constrain the end-members in the mixing analysis.
557 Nevertheless, our one-month field experiment demonstrates the marked short-term variability of several natural
558 tracers in a small, highly dynamic watershed. The hydrograph separation exercise clearly showed that long-
559 term, high-frequency isotopic and chemical analyses are essential for capturing the "unusual but informative"
560 events that shed light on catchment storage and flow processes. We further showed that the right timing for
561 capturing peak event-water contributions can easily be missed with conventional grab sampling strategies,
562 resulting in an underestimation of the event-water fraction. In addition, the relative timing of the isotopic and
563 chemical responses was highly variable, demonstrating the challenge of capturing the right moments with
564 episodic snapshot campaigns or long-term monitoring with daily, weekly, or even monthly sampling intervals.

565

566 As was shown here and elsewhere (e.g., Kirchner, 2003), short-term responses of streamflow and environmental
567 tracers may follow distinctly different patterns, which helps in constraining streamflow-generating mechanisms
568 and quantifying short transit times. Thus, high-frequency isotopic and chemical measurements also have great
569 potential for catchment model validation. Potential future applications of the system could include sites with
570 rapid hydrologic responses, such as urban streams (e.g., Jarden et al., 2016; Jefferson et al., 2015; Soulsby et
571 al., 2014), wastewater- and drinking water systems (e.g., Houhou et al., 2010; Kracht et al., 2007) or agricultural
572 catchments with artificial drainage networks (e.g., Doppler et al., 2012; Heinz et al., 2014).



573 **Acknowledgements**

574 We thank Anton Burkhardt and the facilities staff of the Swiss Federal Institute for Forest, Snow and Landscape
575 Research (WSL) for logistical support, and Matthias Haeni from the Long-term Forest Ecosystem Research
576 Programme (LWF) at WSL for providing air temperature data. We also would like to thank Kate Dennis and
577 David Kim-Hak of Picarro Inc. (Santa Clara, CA, USA) for technical advice.



References

- Aubert, A. H., Gascuel-Oudou, C., Gruau, G., Akkal, N., Faucheux, M., Fauvel, Y., Grimaldi, C., Hamon, Y., Jaffrezic, A., Lecoz-Boutnik, M., Molenat, J., Petitjean, P., Ruiz, L., and Merot, P.: Solute transport dynamics in small, shallow groundwater-dominated agricultural catchments: insights from a high-frequency, multisolute 10 yr-long monitoring study, *Hydrol. Earth Syst. Sci.*, 17, 1379-1391, 10.5194/hess-17-1379-2013, 2013.
- Benettin, P., Kirchner, J. W., Rinaldo, A., and Botter, G.: Modeling chloride transport using travel time distributions at Plynlimon, Wales, *Water Resour. Res.*, 51, 3259-3276, 10.1002/2014WR016600, 2015.
- Berman, E. S. F., Gupta, M., Gabrielli, C., Garland, T., and McDonnell, J. J.: High-frequency field-deployable isotope analyzer for hydrological applications, *Water Resour. Res.*, 45, 10.1029/2009wr008265, 2009.
- 10 Buso, D. C., Likens, G. E., and Eaton, J. S.: Chemistry of precipitation, streamwater, and lakewater from the Hubbard Brook Ecosystem Study: a record of sampling protocols and analytical procedures., USDA Forest Service, Northeastern Research Station Gen. Tech. Rep. NE-275. 52 pp. USDA Forest Service, Newtown Square, PA., 2000.
- Darling, W. G., and Bowes, M. J.: A long-term study of stable isotopes as tracers of processes governing water flow and quality in a lowland river basin: the upper Thames, UK, *Hydrol. Process.*, 30, 2178-2195, 10.1002/hyp.10779, 2016.
- 15 Doppler, T., Camenzuli, L., Hirzel, G., Krauss, M., Luck, A., and Stamm, C.: Spatial variability of herbicide mobilisation and transport at catchment scale: insights from a field experiment, *Hydrol. Earth Syst. Sci.*, 16, 1947-1967, 10.5194/Hess-16-1947-2012, 2012.
- Dzikowski, M., and Jobard, S.: Mixing law versus discharge and electrical conductivity relationships: application to an alpine proglacial stream, *Hydrol. Process.*, 26, 2724-2732, Doi 10.1002/Hyp.8366, 2012.
- 20 Fischer, B. M. C., Rinderer, M., Schneider, P., Ewen, T., and Seibert, J.: Contributing sources to baseflow in pre-alpine headwaters using spatial snapshot sampling, *Hydrol. Process.*, 10.1002/hyp.10529, 2015.
- Genereux, D.: Quantifying uncertainty in tracer-based hydrograph separations, *Water Resour. Res.*, 34, 915-919, 1998.
- GIS-ZH: Geographisches Informationssystem des Kantons Zürich (GIS-ZH), Amt für Raumentwicklung, Abteilung Geoinformation, GIS-Produkte GIS-Browser (Map: Bodenkarte der Landwirtschaftsflächen / <http://maps.zh.ch/> / 4 October 2016), 2016.
- 25 Gupta, P., Noone, D., Galewsky, J., Sweeney, C., and Vaughn, B. H.: Demonstration of high-precision continuous measurements of water vapor isotopologues in laboratory and remote field deployments using wavelength-scanned cavity ring-down spectroscopy (WS-CRDS) technology, *Rapid Commun Mass Sp*, 23, 2534-2542, 10.1002/rcm.4100, 2009.
- Halliday, S. J., Skeffington, R. A., Wade, A. J., Neal, C., Reynolds, B., Norris, D., and Kirchner, J. W.: Upland streamwater nitrate dynamics across decadal to sub-daily timescales: a case study of Plynlimon, Wales, *Biogeosciences*, 10, 8013-8038, 2013.
- 30 Hangen, E., Lindenlaub, M., Leibundgut, C., and von Wilpert, K.: Investigating mechanisms of stormflow generation by natural tracers and hydrometric data: a small catchment study in the Black Forest, Germany, *Hydrol. Process.*, 15, 183-199, 2001.
- Harman, C. J.: Time-variable transit time distributions and transport: Theory and application to storage-dependent transport of chloride in a watershed, *Water Resour. Res.*, 51, 1-30, 10.1002/2014WR015707, 2015.
- Hayashi, M., Vogt, T., Mächler, L., and Schirmer, M.: Diurnal fluctuations of electrical conductivity in a pre-alpine river: Effects of photosynthesis and groundwater exchange, *Journal of Hydrology*, 450, 93-104, Doi 10.1016/J.jhydrol.2012.05.020, 2012.



- Heinz, E., Kraft, P., Buchen, C., Frede, H. G., Aquino, E., and Breuer, L.: Set Up of an Automatic Water Quality Sampling System in Irrigation Agriculture, *Sensors-Basel*, 14, 212-228, 10.3390/S140100212, 2014.
- Herbstritt, B., Gralher, B., and Weiler, M.: Continuous in situ measurements of stable isotopes in liquid water, *Water Resour. Res.*, 48, 10.1029/2011wr011369, 2012.
- 5 Houhou, J., Lartiges, B. S., France-Lanord, C., Guilmette, C., Poix, S., and Mustin, C.: Isotopic tracing of clear water sources in an urban sewer: A combined water and dissolved sulfate stable isotope approach, *Water Research*, 44, 256-266, 10.1016/j.watres.2009.09.024, 2010.
- Jarden, K. M., Jefferson, A. J., and Grieser, J. M.: Assessing the effects of catchment-scale urban green infrastructure retrofits on hydrograph characteristics, *Hydrol. Process.*, 30, 1536-1550, 10.1002/hyp.10736, 2016.
- 10 Jasechko, S., Kirchner, J. W., Welker, J. M., and McDonnell, J. J.: Substantial proportion of global streamflow less than three months old, *Nature Geoscience*, 9, 126-129, 10.1038/Ngeo2636, 2016.
- Jefferson, A. J., Bell, C. D., Clinton, S. M., and McMillan, S. K.: Application of isotope hydrograph separation to understand contributions of stormwater control measures to urban headwater streams, *Hydrol. Process.*, 29, 5290-5306, 10.1002/hyp.10680, 2015.
- Kendall, C., and McDonnell, J. J.: *Isotope tracers in catchment hydrology*, Elsevier, Amsterdam ; New York, xxix, 839 p. pp., 1998.
- 15 Kirchner, J. W.: A double paradox in catchment hydrology and geochemistry, *Hydrol. Process.*, 17, 871-874, 10.1002/Hyp.5108, 2003.
- Kirchner, J. W., Feng, X. H., Neal, C., and Robson, A. J.: The fine structure of water-quality dynamics: the (high-frequency) wave of the future, *Hydrol. Process.*, 18, 1353-1359, 10.1002/Hyp.5537, 2004.
- Kirchner, J. W., and Neal, C.: Universal fractal scaling in stream chemistry and its implications for solute transport and water quality trend detection, *P Natl Acad Sci USA*, 110, 12213-12218, 10.1073/Pnas.1304328110, 2013.
- 20 Klaus, J., and McDonnell, J. J.: Hydrograph separation using stable isotopes: Review and evaluation, *Journal of Hydrology*, 505, 47-64, 10.1016/j.jhydrol.2013.09.006, 2013.
- Kracht, O., Gresch, M., and Gujer, W.: A Stable Isotope Approach for the Quantification of Sewer Infiltration, *Environmental Science & Technology*, 41, 5839-5845, 10.1021/es062960c, 2007.
- 25 Leibundgut, C., and Seibert, J.: Tracer Hydrology, in: *The Science of Hydrology*, edited by: Uhlenbrook, S., *Treatise on Water Science*, Elsevier, Amsterdam, 215-236, 2011.
- Lyon, S. W., Desilets, S. L. E., and Troch, P. A.: Characterizing the response of a catchment to an extreme rainfall event using hydrometric and isotopic data, *Water Resour. Res.*, 44, 10.1029/2007wr006259, 2008.
- Lyon, S. W., Desilets, S. L. E., and Troch, P. A.: A tale of two isotopes: differences in hydrograph separation for a runoff event when using delta D versus delta O-18, *Hydrological Processes*, 23, 2095-2101, 10.1002/hyp.7326, 2009.
- 30 Matsubayashi, U., Velasquez, G. T., and Takagi, F.: Hydrograph separation and flow analysis by specific electrical conductance of water, *Journal of Hydrology*, 152, 179-199, 10.1016/0022-1694(93)90145-Y, 1993.
- McClain, E. M., Boyer, W. E., Dent, L. C., Gergel, E. S., Grimm, B. N., Groffman, M. P., Hart, C. S., Harvey, W. J., Johnston, A. C., Mayorga, E., McDowell, H. W., and Pinay, G.: Biogeochemical Hot Spots and Hot Moments at the Interface of Terrestrial and Aquatic Ecosystems, *Ecosystems*, 6, 301-312, 10.1007/s10021-003-0161-9, 2003.
- 35 McDonnell, J. J., Bonell, M., Stewart, M. K., and Pearce, A. J.: Deuterium Variations in Storm Rainfall - Implications for Stream Hydrograph Separation, *Water Resour. Res.*, 26, 455-458, 10.1029/WR026i003p00455, 1990.



- McGlynn, B. L., and McDonnell, J. J.: Quantifying the relative contributions of riparian and hillslope zones to catchment runoff, *Water Resour. Res.*, 39, 10.1029/2003wr002091, 2003.
- Munksgaard, N. C., Wurster, C. M., and Bird, M. I.: Continuous analysis of delta O-18 and delta D values of water by diffusion sampling cavity ring-down spectrometry: a novel sampling device for unattended field monitoring of precipitation, ground and surface waters, *Rapid Commun Mass Sp*, 25, 3706-3712, 10.1002/rcm.5282, 2011.
- Munksgaard, N. C., Wurster, C. M., Bass, A., and Bird, M. I.: Extreme short-term stable isotope variability revealed by continuous rainwater analysis, *Hydrol. Process.*, 26, 3630-3634, 10.1002/hyp.9505, 2012.
- Muñoz-Villers, L. E., and McDonnell, J. J.: Runoff generation in a steep, tropical montane cloud forest catchment on permeable volcanic substrate, *Water Resour. Res.*, 48, n/a-n/a, 10.1029/2011WR011316, 2012.
- 10 Neal, C., Reynolds, B., Norris, D., Kirchner, J. W., Neal, M., Rowland, P., Wickham, H., Harman, S., Armstrong, L., Sleep, D., Lawlor, A., Woods, C., Williams, B., Fry, M., Newton, G., and Wright, D.: Three decades of water quality measurements from the Upper Severn experimental catchments at Plynlimon, Wales: an openly accessible data resource for research, modelling, environmental management and education, *Hydrol. Process.*, 25, 3818-3830, 10.1002/hyp.8191, 2011.
- 15 Neal, C., Reynolds, B., Rowland, P., Norris, D., Kirchner, J. W., Neal, M., Sleep, D., Lawlor, A., Woods, C., Thacker, S., Guyatt, H., Vincent, C., Hockenhull, K., Wickham, H., Harman, S., and Armstrong, L.: High-frequency water quality time series in precipitation and streamflow: From fragmentary signals to scientific challenge, *Sci Total Environ*, 434, 3-12, <http://dx.doi.org/10.1016/j.scitotenv.2011.10.072>, 2012.
- Pangle, L. A., Klaus, J., Berman, E. S. F., Gupta, M., and McDonnell, J. J.: A new multisource and high-frequency approach to measuring $\delta^2\text{H}$ and $\delta^{18}\text{O}$ in hydrological field studies, *Water Resour. Res.*, 49, 7797-7803, 10.1002/2013WR013743, 2013.
- 20 Pellerin, B. A., Wollheim, W. M., Feng, X., and Vörörsmarty, C. J.: The application of electrical conductivity as a tracer for hydrograph separation in urban catchments, *Hydrol. Process.*, 22, 1810-1818, 10.1002/hyp.6786, 2008.
- Pinder, G. F., and Jones, J. F.: Determination of the ground-water component of peak discharge from the chemistry of total runoff, *Water Resour. Res.*, 5, 438-445, 10.1029/WR0051002p00438, 1969.
- 25 Richey, D. G., McDonnell, J. J., Erbe, M. W., and Hurd, T. M.: Hydrograph separations based on chemical and isotopic concentrations: A critical appraisal of published studies from New Zealand, North America and Europe, *Journal of Hydrology New Zealand*, 37, 95-111, 1998.
- Riml, J., and Worman, A.: Spatiotemporal decomposition of solute dispersion in watersheds, *Water Resour. Res.*, 51, 2377-2392, 10.1002/2014WR016385, 2015.
- 30 Rode, M., Angelstein, S. H. N., Anis, M. R., Borchardt, D., and Weitere, M.: Continuous In-Stream Assimilatory Nitrate Uptake from High Frequency Sensor Measurements, *Environmental Science & Technology*, 50, 5685-5694, 2016a.
- Rode, M., Wade, A. J., Cohen, M. J., Hensley, R. T., Bowes, M. J., Kirchner, J. W., Arhonditsis, G. B., Jordan, P., Kronvang, B., Halliday, S. J., Skeffington, R. A., Rozemeijer, J. C., Aubert, A. H., Rinke, K., and Jomaa, S.: Sensors in the Stream: The High-Frequency Wave of the Present, *Environmental Science & Technology*, 50, 10297-10307, 10.1021/acs.est.6b02155, 2016b.
- 35 Schaub, M., Dobbertin, M., Krauchi, N., and Dobbertin, M. K.: Preface-long-term ecosystem research: understanding the present to shape the future, *Environ Monit Assess*, 174, 1-2, 2011.
- Soulsby, C., Birkel, C., and Tetzlaff, D.: Assessing urbanization impacts on catchment transit times, *Geophysical Research Letters*, 41, 442-448, 2014.
- Sposito, G.: *The chemistry of soils*, 2nd ed., Oxford University Press, Oxford; New York, xii, 329 p. pp., 2008.



Tetzlaff, D., Birkel, C., Dick, J., Geris, J., and Soulsby, C.: Storage dynamics in hydrogeological units control hillslope connectivity, runoff generation, and the evolution of catchment transit time distributions, *Water Resour. Res.*, 50, 969-985, 2014.

5 Vidon, P., Allan, C., Burns, D., Duval, T. P., Gurwick, N., Inamdar, S., Lowrance, R., Okay, J., Scott, D., and Sebestyen, S.: Hot Spots and Hot Moments in Riparian Zones: Potential for Improved Water Quality Management, *JAWRA Journal of the American Water Resources Association*, 46, 278-298, 10.1111/j.1752-1688.2010.00420.x, 2010.

Vitvar, T., and Balderer, W.: Estimation of mean water residence times and runoff generation by O-18 measurements in a pre-Alpine catchment (Rietholzbach, eastern Switzerland), *Applied Geochemistry*, 12, 787-796, 1997.

10 Weiler, M., Scherrer, S., Naef, F., and Burlando, P.: Hydrograph separation of runoff components based on measuring hydraulic state variables, tracer experiments, and weighting methods, *Integrated Methods in Catchment Hydrology: Tracer, Remote Sensing and New Hydrometric Techniques*, 249-255, 1999.

Wels, C., Cornett, R. J., and Lazerte, B. D.: Hydrograph Separation - a Comparison of Geochemical and Isotopic Tracers, *Journal of Hydrology*, 122, 253-274, 10.1016/0022-1694(91)90181-G, 1991.



Tables

Table 1: Average isotope values and solute concentrations, as well as standard deviations (and relative standard deviations RSD) of three water samples analyzed during two different 48h experiments with the isotope analyzer and IC, respectively. In Fiji bottled water, diluted tap water and nanopure water, concentrations of F^- , Li^+ , K^+ , NH_4^+ and PO_4^{3-} were mostly below the LOQ, and thus were not included in the table. The calculation of the average memory coefficient is described in the text (Eq. (1)). The uncertainties of the IC measurements were obtained by simple linear regression analysis of the average value and the standard deviation of the respective constituent.

	Isotope laboratory experiment		IC laboratory experiment					
	$\delta^{18}O$	δ^2H	Na^+	Mg^{2+}	Ca^{2+}	Cl^-	NO_3^-	SO_4^{2-}
Limit of quantification (LOQ) (mg L ⁻¹)	-	-	0.1	0.1	0.1	0.05	0.05	0.05
Measurement uncertainty (%) or (mg L ⁻¹)	0.03	0.17	0.053+ 0.005-C	0.008+ 0.006-C	0.087+ 0.009-C	0.027+ 0.003-C	0.028+ 0.002-C	0.037+ 0.006-C
Water sample	Fiji bottled water		Fiji bottled water					
Number of measurements	12	12	10	10	10	10	10	10
Average value (‰) or (mg L ⁻¹)	-4.86	-35.89	21.6	15.7	24.3	9.69	1.05	1.56
Standard deviation (‰) or (mg L ⁻¹)	0.06	0.26	0.1	0.1	0.3	0.06	0.05	0.03
RSD (%)	-	-	0.5	0.4	1.1	0.60	4.3	1.80
Linear drift ((‰ 24h ⁻¹) or (mg L ⁻¹ 24h ⁻¹))	-0.009±0.008	0.133±0.040	0.129± 0.056 ^a	0.058± 0.036 ^b	0.093± 0.160 ^c	0.088± 0.019	-0.078± 0.008	0.045± 0.007
Water sample	Tap water		Diluted tap water					
Number of measurements	34	34	17	18	18	18	18	18
Average value (‰) or (mg L ⁻¹)	-9.40	-68.55	10.9	34.4	133.2	12.41	4.96	17.29
Standard deviation (‰) or (mg L ⁻¹)	0.03	0.12	0.1	0.2	1.3	0.057	0.03	0.14
RSD (%)	-	-	0.7	0.6	1.0	0.5	0.7	0.8
Water sample	Nanopure water		Nanopure water (last sample)					
Number of measurements	43	43	27	27	27	27	27	27
Average value (‰) or (mg L ⁻¹)	-9.44	-68.67	<LOQ	0.1	0.6	<LOQ	<LOQ	0.09
Standard deviation (‰) or (mg L ⁻¹)	0.02	0.18	0.02	0.003	0.1	0.03	0.02	0.05
Carryover (%)	0.9	1.2	2.8	3.3	3.8	2.1	1.9	2.3

^a p > 0.05^b p > 0.15^c p > 0.50



Table 2: Characteristics of precipitation events and antecedent moisture conditions during the field experiment. Initial stream stage is used here as a proxy for initial discharge.

Event	Start of event	Total precipitation (mm)	Total precipitation until peak flow (mm)	Response time (h)	48h antecedent precipitation (mm)	24h antecedent precipitation (mm)	Initial stream stage (cm)
#1	14 February 2016 10:30	6.7	5.1	01:40	8.5	2.9	0.44
#2	20 February 2016 12:30	10.3	9.2	00:00	1.3	0.0	0.36
#3	23 February 2016 07:00	5.0	4.8	00:00	0.2	0.2	0.37
#4	24 February 2016 15:30	15.3	11.1	01:00	5.2	3.3	0.41
#5	28 February 2016 05:50	10.6	2.9	01:10	0.0	0.0	0.38
#6	02 March 2016 12:30	6.0	6.0	01:50	11.9	2.0	0.46
#7	05 March 2016 05:20	9.4	8.6	01:30	4.3	0.9	0.45
#8	07 March 2016 21:00	6.4	6.4	04:00	1.9	0.0	0.45



Figures

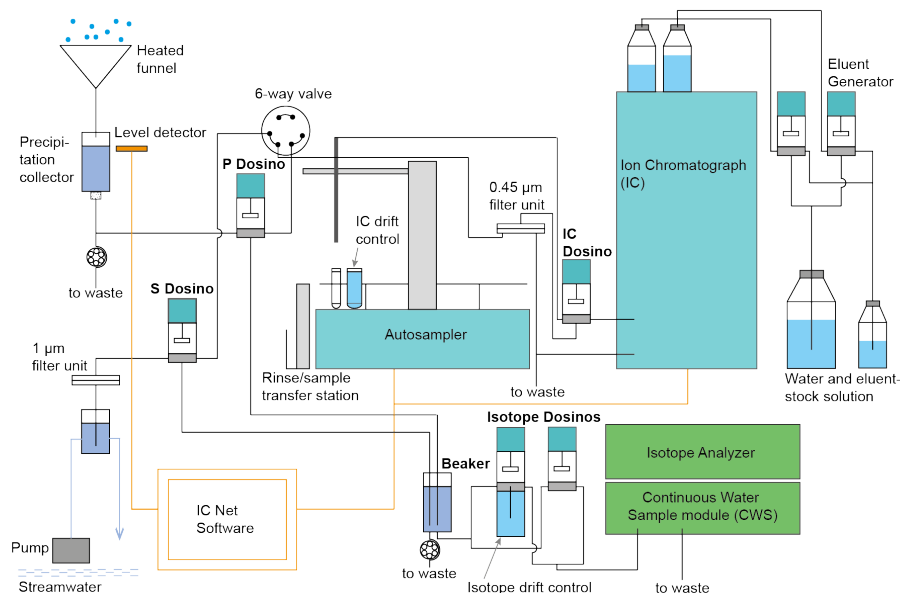


Figure 1: Schematic overview of the coupled isotope analyzer / IC- system for the collection and measurement of streamwater and precipitation samples. Components of the sample distribution and the IC are shown in blue color, while the isotope analyzer with CWS is shown in green color.

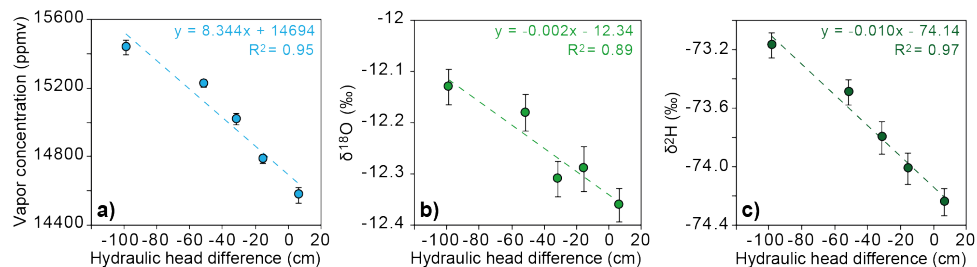


Figure 2: Measured vapor concentrations (panel a)), and isotope ratios (panels b) and c)) of a single water sample (nanopure water) as a function of the hydraulic head difference between the water level in the sample bottle and the waste outlet of the CWS. Negative values of the hydraulic head difference indicate that the sample source was located below the waste outlet of the CWS.

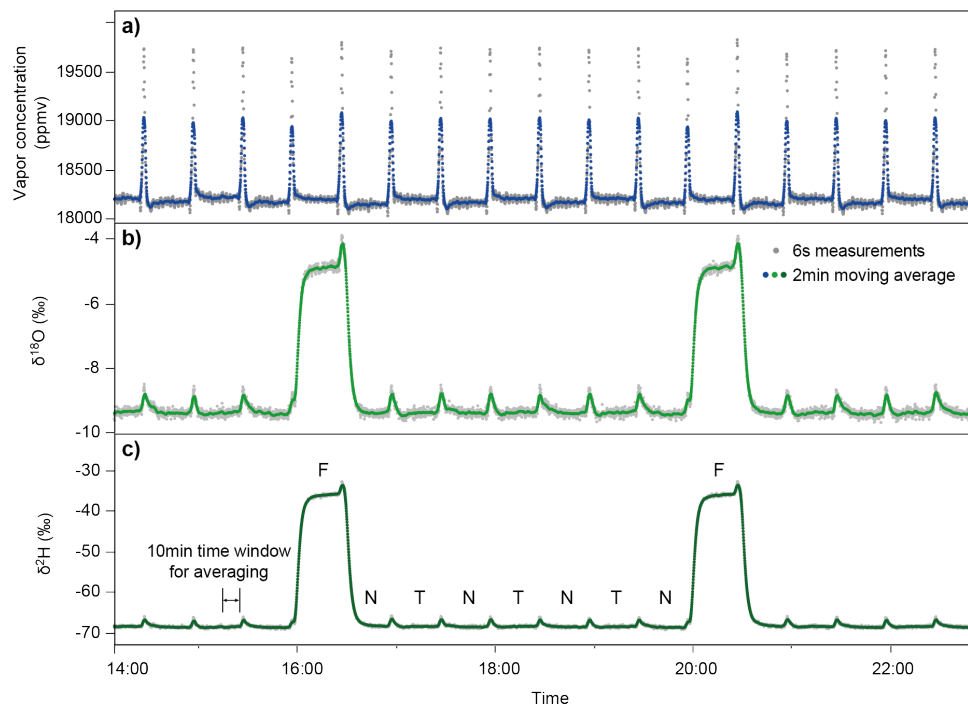


Figure 3: Nine hour excerpt showing vapor concentrations (panel a) and isotope measurements (panels b) and c) in tap water (T), nanopure water (N) and Fiji bottled water (F) during the 48h laboratory experiment. Samples were injected alternately with two Dosinos for 30min each at a flow rate of 1 mL min^{-1} .

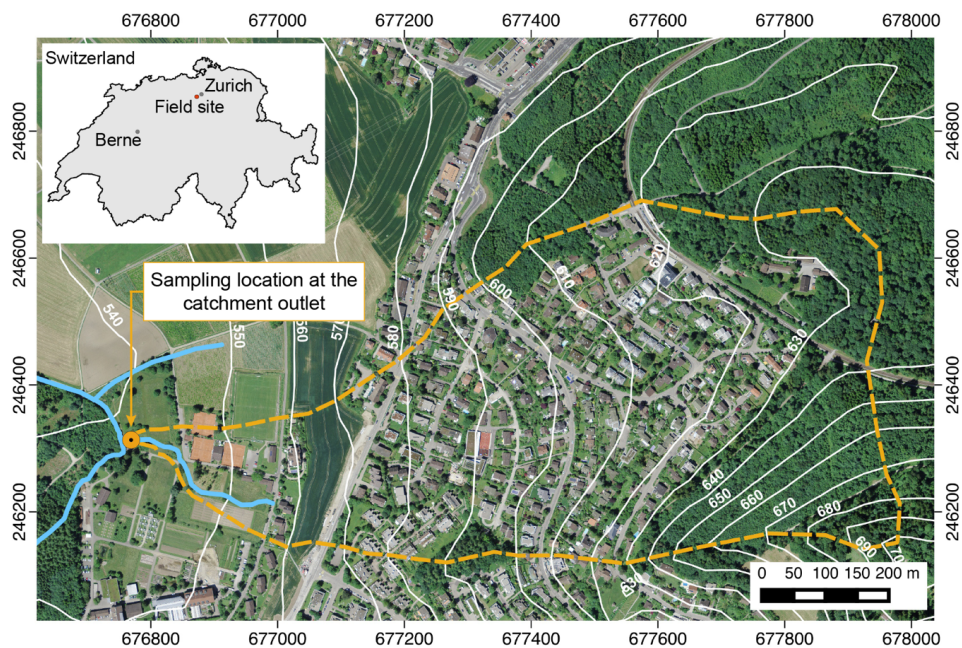
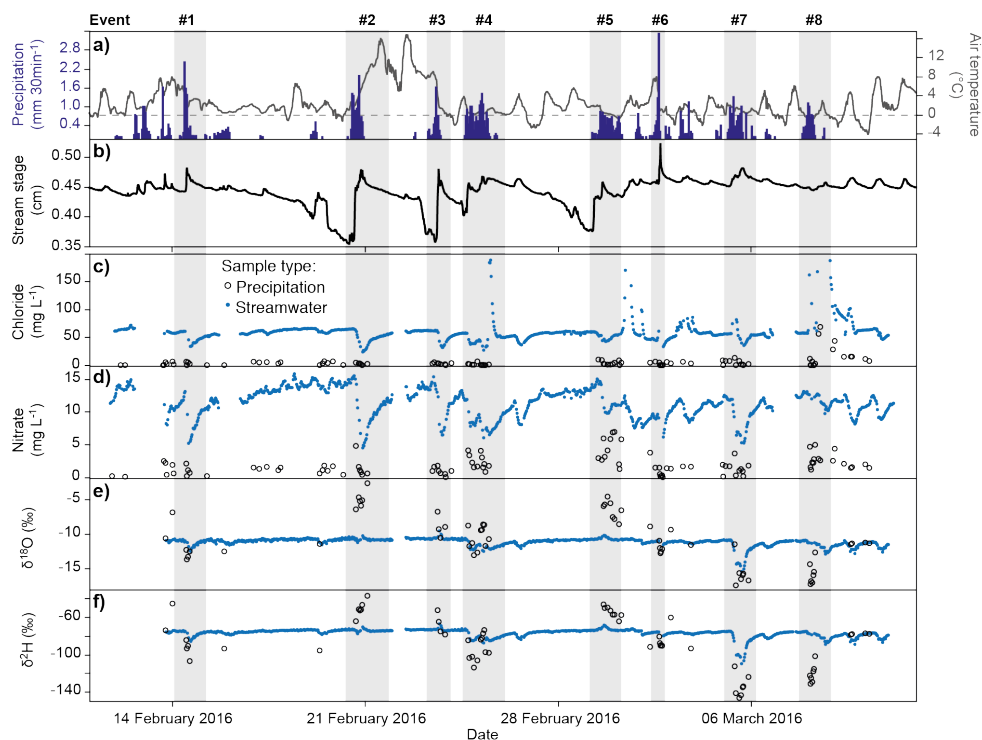


Figure 4: Location of the field site at a small creek on the property of the Swiss Federal Institute for Forest, Snow and Landscape Research (WSL) near Zurich, Switzerland. Catchment boundaries are approximate.



5 **Figure 5:** Time series of precipitation, air temperature (a) and stream stage (b) at the field site during the four-week study period. Panels c) and d) show the chloride and nitrate concentrations, whereas panels e) and f) show the isotopic compositions. Streamwater samples are shown by blue dots and precipitation samples are shown by open circles. Vertical grey bars indicate the periods of the eight precipitation events used for hydrograph separation.

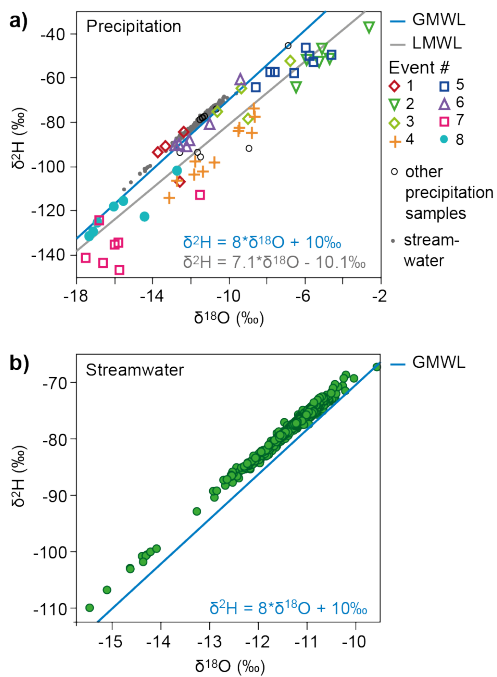
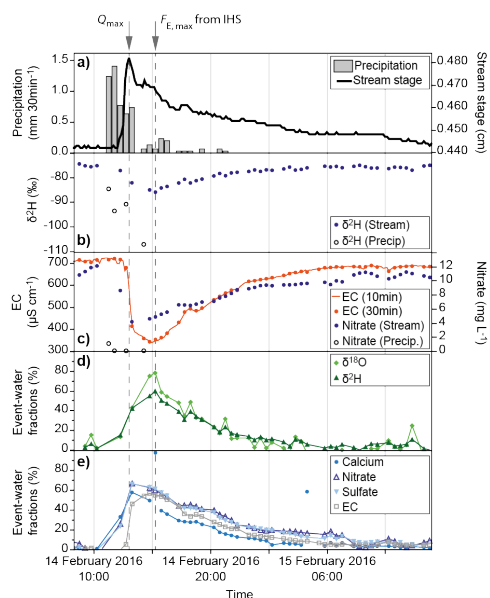


Figure 6: Dual-isotope plot of all $\delta^{18}\text{O}$ and $\delta^2\text{H}$ values measured in precipitation (a) and streamwater (b) during the field experiment. Streamwater samples are also plotted in grey in the upper panel for comparison (note the difference in scales). The global meteoric water line (GMWL) and the linear fit to the precipitation data (local meteoric water line, LMWL) are shown in blue and in grey, respectively.

5



5 **Figure 7: Precipitation Event #1 together with the hydrologic (a), isotopic (b) and chemical (c) responses in streamwater. Panels d) and e) show the fractions of event-water based on isotopic and chemical hydrograph separation, respectively, which are similar for both types of tracers. However, the timing of the maximum event-water fraction ($F_{E,max}$) differs, i.e. the isotopes indicate the largest contribution of event water around 2h after the flood peak (Q_{max}) was reached. In panel e), gaps in the F_E time series based on calcium concentrations are due to measurement outliers.**

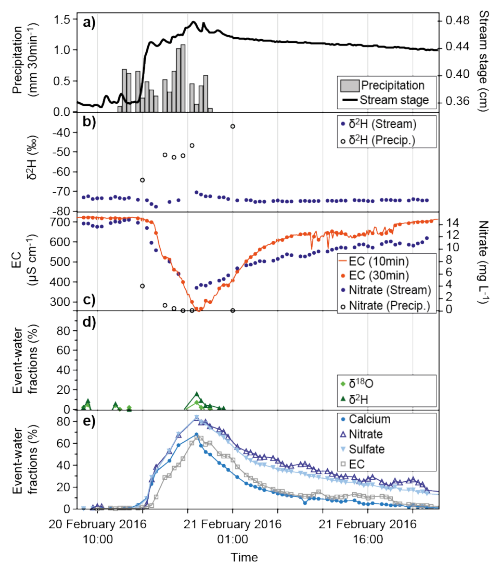


Figure 8: Precipitation Event #2 and the hydrologic, isotopic and chemical responses in streamwater. Panels d) and e) show the fractions of event water (F_E) based on isotopic and chemical hydrograph separation. Chemical tracers greatly exaggerate the event-water fraction.

5

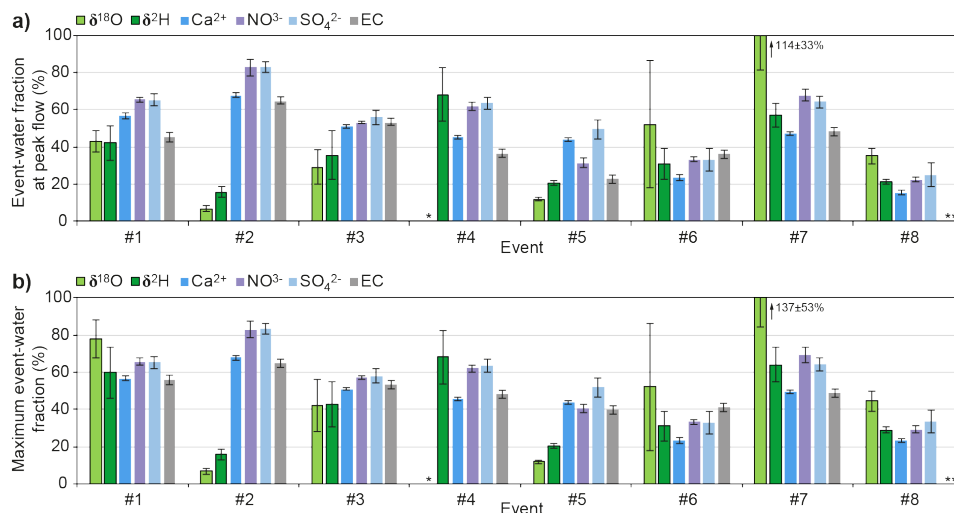


Figure 9: Event-water fractions (F_E) based on isotopic and chemical hydrograph separation for eight storm events. Panel a) shows F_E during peak flow, and panel b) shows the maximum event-water fractions ($F_{E,\max}$) of each event. Unrealistic F_E and $F_{E,\max}$ values were obtained for Event #4 based on $\delta^{18}\text{O}$ because the isotopic signatures in precipitation and pre-event streamwater were too similar (*). For Event #8, wash-off of road salt resulted in unrealistic F_E and $F_{E,\max}$ values based on EC, i.e. $-95\pm 7\%$ (**).

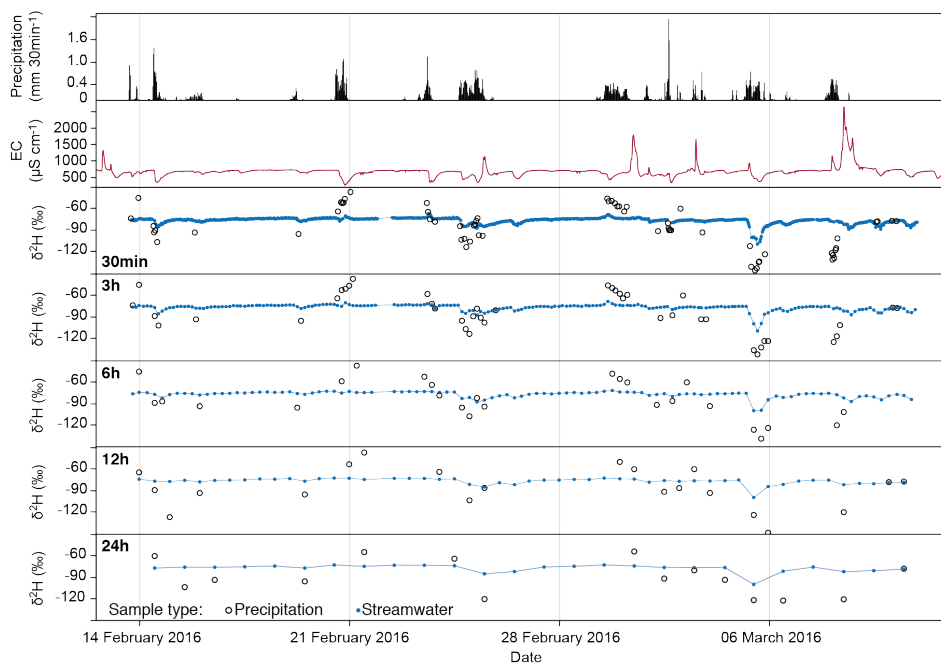


Figure 10: Time series of precipitation and streamwater EC (at 10min temporal resolution), as well as $\delta^2\text{H}$ values in streamwater and precipitation at sampling intervals of 30min, 3h, 6h, 12h and 24h.

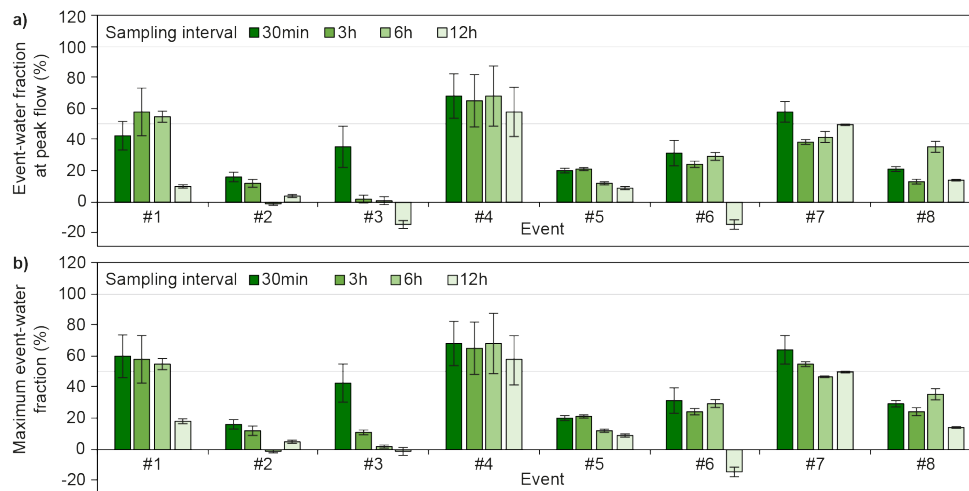


Figure 11: Event-water fractions at peak flow (a) and maximum event-water fractions (b) based on $\delta^2\text{H}$ measurements at sampling intervals of 30min, 3h, 6h and 12h. With lower sampling frequencies, the event-water fractions are often underestimated or become even unrealistic, as the likelihood increases that the point of largest $\delta^2\text{H}$ variations in streamflow will be missed.